

# A General Carboxylate-Assisted Approach to Boost the ORR Performance of ZIF-Derived Fe/N/C Catalysts for Proton Exchange Membrane Fuel Cells

Yuyang Li, Pengyang Zhang, Liyang Wan, Yanping Zheng, Ximing Qu, Haikun Zhang, Yuesheng Wang, Karim Zaghib, Jiayin Yuan, Shuhui Sun, Yucheng Wang,\* Zhiyou Zhou,\* and Shigang Sun

An Fe/N/C catalyst derived from the pyrolysis of metal–organic frameworks, for example, a zeolitic-imidazolate-framework-8 (ZIF-8), has been regarded as one of the most promising non-precious metal catalysts toward oxygen reduction reaction (ORR) in proton exchange membrane fuel cells (PEMFCs). However, its ORR mass activity is still much inferior to that of Pt, partly because of the lack of general and efficient synthetic strategies. Herein, a general carboxylate-assisted strategy that dramatically enhances the ORR mass activity of ZIF-derived Fe/N/C catalysts is reported. The carboxylate is found to promote the formation of Fe/N/C catalysts with denser accessible active sites and entangled carbon nanotubes, as well as a higher mesoporosity. These structural advantages make the carboxylate-assisted Fe/N/C catalysts show a 2–10 fold higher ORR mass activity than the common carboxylate-free one in various cases. When applied in H<sub>2</sub>–O<sub>2</sub> PEMFCs, the active acetate-assisted Fe/N/C catalyst generates a peak power density of 1.33 W cm<sup>-2</sup>, a new record of peak power density for a H<sub>2</sub>–O<sub>2</sub> PEMFC with non-Pt ORR catalysts.

been made in the synthesis of high-performance M/N/C catalysts.<sup>[1]</sup> Among various types of metal centers, Fe/N/C catalyst with Fe as the metal center has been demonstrated to be the most active one,<sup>[2]</sup> the ORR mass activity of which is however still much inferior to that of Pt/C. To achieve a current density comparable to the Pt/C cathode in the kinetic region (high cell voltage or low current density) under PEMFC working conditions, a tenfold catalyst loading in Fe/N/C cathode, typical at a loading level of 4 mg cm<sup>-2</sup>, is required.<sup>[3]</sup> Nevertheless, such a high loading causes a severe problem for mass-transfer in a high current density region, and consequently a low peak power density ( $P_{\max}$ ).<sup>[4]</sup> As such, the ORR mass activity of Fe/N/C catalysts should be improved further, which is rather challenging.


The pyrolysis of metal–organic frameworks, for example, a zeolitic-imidazolate-framework-8 (ZIF-8), is an effective strategy to develop active M/N/C catalysts.<sup>[3a,5]</sup> The optimization of synthetic conditions, for example, the types, content, and distribution of metal ions in the ZIF-8 precursors,<sup>[5a,6]</sup> the ZIF-8 particle size, pyrolysis temperature, and atmosphere,<sup>[3a,7]</sup> can easily position these ZIF-based catalysts among the best non-precious metal ORR catalysts. For further improving the ORR activity of these ZIF-based

## 1. Introduction

Pyrolyzed metal/nitrogen/carbon (M/N/C) materials have been considered as the most promising non-precious catalyst to replace the state-of-the-art Pt catalysts for oxygen reduction reaction (ORR) in proton exchange membrane fuel cells (PEMFCs). With substantial effort, remarkable progress has

Y. Li, P. Zhang, L. Wan, Dr. Y. Zheng, X. Qu, H. Zhang, Prof. Y. Wang, Prof. Z. Zhou, Prof. S. Sun  
State Key Laboratory of Physical Chemistry of Solid Surfaces  
Collaborative Innovation Center of Chemistry for Energy Materials  
College of Chemistry and Chemical Engineering  
Xiamen University  
Xiamen 361005, China  
E-mail: wangyc@xmu.edu.cn; zhouzy@xmu.edu.cn  
Dr. Y. Wang, K. Zaghib  
Center of Excellence in Transportation Electrification and Energy Storage  
Hydro Québec  
Varenes, Québec J3X 1S1, Canada

Prof. J. Yuan  
Department of Materials and Environmental Chemistry  
Stockholm University  
Stockholm 10691, Sweden  
Prof. S. Sun  
Institut National de la Recherche Scientifique-Énergie  
Matériaux et Télécommunications  
Varenes, Québec J3X 1S2, Canada  
Prof. Y. Wang, Prof. Z. Zhou  
Innovation Laboratory for Sciences and Technologies  
of Energy Materials of Fujian Province (IKKEM)  
Xiamen 361005, China

 The ORCID identification number(s) for the author(s) of this article can be found under <https://doi.org/10.1002/adfm.202009645>.

DOI: 10.1002/adfm.202009645

catalysts more efficient strategies are needed. Additionally, the general applicability of the methods is equally critical. However, such strategies have only been reported in a few cases. For example, Shui and co-workers used mesoporous SiO<sub>2</sub> to enhance ZIF-derived catalysts' ORR activity by increasing the density of accessible active sites and decreasing mass-transport loss.<sup>[8]</sup> Wu and co-workers developed a carbon-shell confinement strategy by using surfactants capping onto ZIF precursors to increase active site density and, consequently a higher ORR activity.<sup>[3c]</sup> So far, efficient and general strategies are still needed and highly desirable for the development of ZIF-based ORR catalysts.

In this study, we reported a carboxylate-assisted general strategy to amplify the ORR mass activity of ZIF-derived Fe/N/C catalysts. The carboxylate increased the Fe doping content in the ZIF-8 precursors, resulting in a higher density of FeN<sub>x</sub> active sites and entangled CNTs in the final pyrolyzed Fe/N/C catalysts. Additionally, as a pore-formation agent, the carboxylate increased the mesoporosity of the Fe/N/C catalysts and exposed more active sites accessible to the ORR. These merits increased the ORR mass activity of ZIF-based Fe/N/C catalysts by 2–10 times in various cases. With the optimized Fe/N/C catalyst as a cathode, the H<sub>2</sub>-O<sub>2</sub> PEMFC generated an unprecedentedly high peak power density ( $P_{\max}$ ) of 1.33 W cm<sup>-2</sup> at a decreased catalyst loading of 3 mg cm<sup>-2</sup>.

## 2. Results and Discussion

The fabrication of ZIF-derived Fe/N/C catalysts consisted of two steps: the synthesis of precursors (Fe-doped ZIF-8 particles) and a follow-up pyrolysis at an optimized temperature of 1000 °C for 1 h under Ar atmosphere (Figure S1, Supporting Information). The enhancement effect of the carboxylate on the ORR activity of Fe/N/C catalysts was assumed to be achieved by affecting the precursors' Fe doping process and the pyrolysis process. Herein, the effect of the carboxylate on the precursors was first examined. Before pyrolysis, acetate (OAc), a classic example of a carboxylate, was introduced into the ZIF-8 precursors by a wet-impregnation method accompanying the Fe-doping process. Briefly, a mixture of ferric chloride (FeCl<sub>3</sub>) and potassium acetate (KOAc) in a methanol solution was added to a slurry dispersion of ZIF-8 particles for 12 h, during which the ions of Fe and OAc were introduced into the ZIF-8 particles. After washing, centrifugation, and vacuum drying, the Fe-doped ZIF-8 precursor containing OAc was collected (termed as Fe-ZIF8-OAc). For comparison, a control sample of ZIF-8 precursor with Fe ions but without OAc (Fe-ZIF8) was prepared similarly. The doping experiment was conducted on four different ZIF-8 particles prepared at different molar ratios of 2-methylimidazole ligand and Zn ion ( $N_{\text{mlm}}/N_{\text{Zn}}$ ) from 2 to 10.

**Figure 1a** shows a suggested Fe-doping mechanism of ZIF-8 particles. Without OAc, Fe ions are doped mainly in a known Fe-imidazole coordination form.<sup>[7b,9]</sup> In the presence of OAc, Fe can be additionally introduced in a form, in which the OAc bridges Fe ions and unsaturated coordinated zinc sites.<sup>[10]</sup> This hypothesis was supported by the Fourier transform infrared spectrum (FTIRS) showing two bands at 1340 and 1580 cm<sup>-1</sup> in the Fe-ZIF8-OAc sample at  $N_{\text{mlm}}/N_{\text{Zn}} = 2$ , corresponding

to the symmetric and anti-symmetric stretching vibration of COO–Zn (Figure 1b).<sup>[11]</sup> At a higher  $N_{\text{mlm}}/N_{\text{Zn}}$  ratio, the two bands' intensity showed an apparent attenuation (Figure S2, Supporting Information), which might be due to more imidazole ligands and thus less unsaturated coordinated zinc sites on the surface of the particles.<sup>[12]</sup> Therefore, it was expected that OAc increased the Fe doping amount, and the largest gain was observed at  $N_{\text{mlm}}/N_{\text{Zn}} = 2$ , a case that has more unsaturated coordinated zinc sites than the rest, three. These assumptions were supported experimentally. As shown in Figure 1c,d, all the Fe-ZIF8-OAc series samples showed a higher O and Fe content than OAc-free Fe-ZIF8 samples at each  $N_{\text{mlm}}/N_{\text{Zn}}$ , and the largest increment was observed at  $N_{\text{mlm}}/N_{\text{Zn}} = 2$ . The simultaneously increased Fe and O contents in the Fe-ZIF8-OAc samples suggest that more Fe was maintained in the final Fe/N/C catalysts by the addition of OAc, very possibly as a linker group. A previous DFT calculation also revealed that the direct substitution of Zn ions with Fe ions that coordinate with a carboxylate is difficult because of a strong interaction between Fe ions and carboxylates,<sup>[13]</sup> suggesting that Fe ions are more likely to be doped with OAc as a linker. XPS unveiled only Fe content on the surface region of particles. The overall Fe content of ZIF-8 particles was examined by inductively coupled plasma-mass spectrometry (ICP-MS). Consistent with the trend displayed in the surface region, the overall Fe content increased by the addition of OAc, and the largest increment occurred at  $N_{\text{mlm}}/N_{\text{Zn}} = 2$  (Figure S3, Supporting Information). Note that, both Fe ions and OAc stayed preferably in the ZIF particles' surface region (Figures S4 and S5, Supporting Information), which might be due to a higher content of unsaturated coordinated zinc or imidazole sites in the surface region than the interior. The enrichment of Fe on the Fe-ZIF8-OAc particles did not result in an uneven distribution of itself, as demonstrated by STEM element mapping (Figure S6, Supporting Information). Besides, in the case of 2mlm, the addition of OAc decreased the size of Fe-ZIF8 particles. At higher mlm content, the size of Fe-ZIF8-OAc particles is slightly larger than that of Fe-ZIF8 particles (Figure S7, Supporting Information). The opposite change of particle size may be due to different roles of a carboxylate in the coordination and deprotonation equilibria at different  $N_{\text{mlm}}/N_{\text{Zn}}$ .<sup>[14]</sup>

With OAc and additional Fe ions being uniformly introduced into the ZIF-8 precursors, the structure and property of the resultant pyrolysis products are expected to be different from, preferentially more favorable than the OAc-free sample. **Figure 2a** compares the N<sub>2</sub> adsorption–desorption isotherms of the resulting Fe/N/C catalysts with and without OAc at  $N_{\text{mlm}}/N_{\text{Zn}} = 4$  (labelled as Fe/N/C(4mlm) and Fe/N/C(4mlm)-OAc, respectively). The Fe/N/C(4mlm) catalyst showed a type-I isotherm with 60% of the adsorption capacity in the low-pressure region below  $P/P_0 < 0.1$ , in support of a typical microporous material with a low amount of mesopores. By contrast, the adsorption capacity of the Fe/N/C(4mlm)-OAc catalyst in the low-pressure region was only 22%, and a remarkable hysteresis loop appeared, indicating relatively less micropores content (<2 nm) but more mesopores (2–50 nm). A quantitative comparison of pore structures was provided by their pore size distribution. As shown in Figure 2b, compared with Fe/N/C(4mlm), the Fe/N/C(4mlm)-OAc catalyst

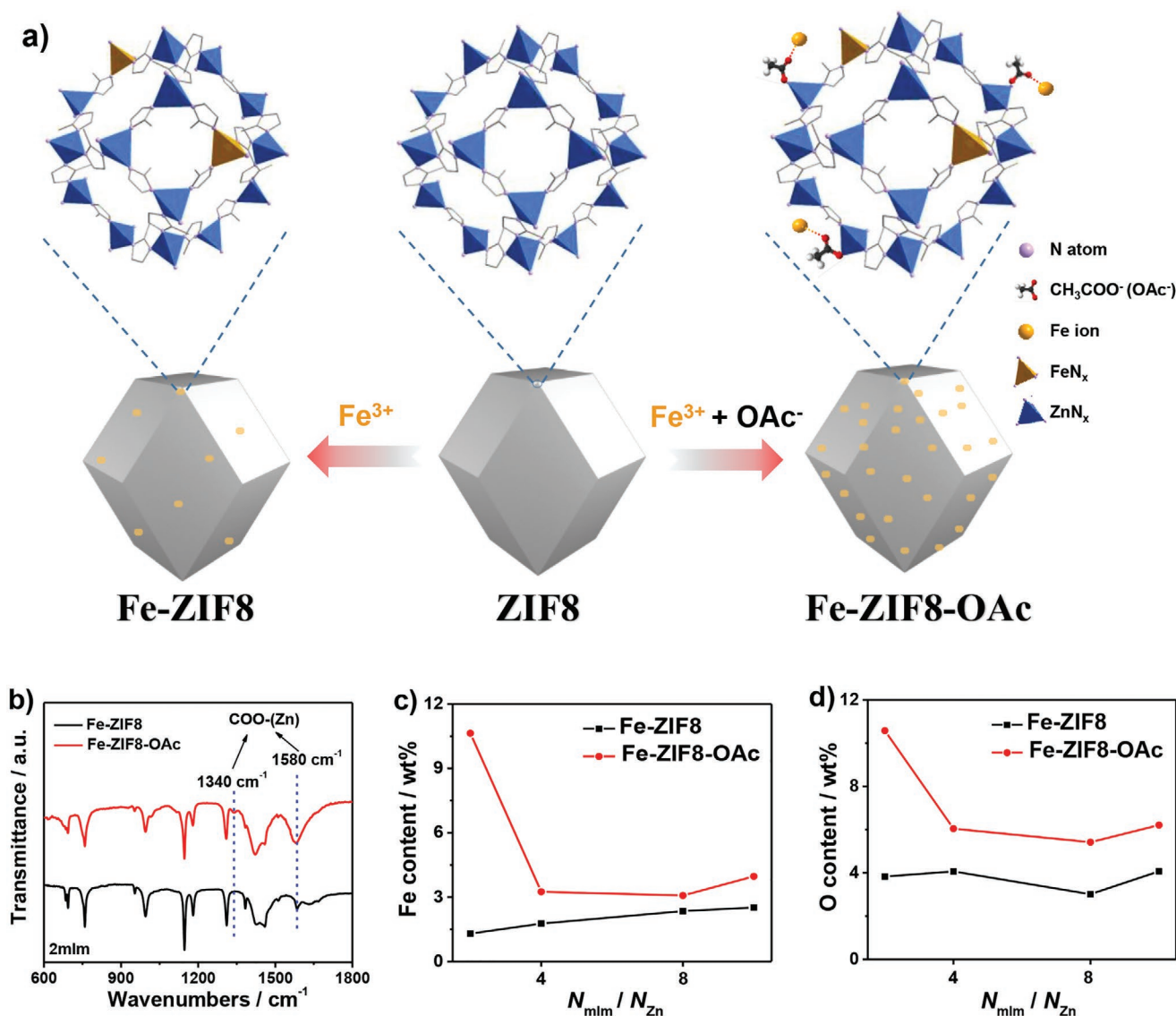


**Figure 1.** a) Schematic diagram of Fe doping mechanisms of ZIF-8 particles with and without OAc; b) FTIR spectra of Fe-ZIF8 and Fe-ZIF8-OAc particles at  $N_{\text{mlm}}/N_{\text{Zn}} = 2$ . c, d) Fe and O content of Fe-ZIF8 and Fe-ZIF8-OAc particles at different  $N_{\text{mlm}}/N_{\text{Zn}}$ . Element content was determined by XPS.

possessed fewer pores at a size smaller than 2.6 nm, but more pores in the range of 2.6 to 100 nm. Similar structure differences between OAc and OAc-free Fe/N/C catalysts were also reflected by their morphologies observed in TEM images. The Fe/N/C(4mlm) catalyst consisted of enclosed polyhedral carbon particles (Figure 2c), while the Fe/N/C(4mlm)-OAc catalyst consisted of open hollow carbon particles with entangled CNTs (Figure 2d and Figure S8, Supporting Information). To clarify OAc's effect on the pore structure, the pyrolysis products of Fe-free ZIF-8 particles doped by different content of OAc were collected, and their pore structures were compared (Figure S9, Supporting Information). It was found that OAc resulted in a decrease of micropores, but an increase of larger pores. This result suggests the loss of pore walls and consequently the merge of smaller pores into larger ones, which is very possibly due to the oxidative corrosion of carbon matrix by OAc during the pyrolysis process.<sup>[15]</sup> Note that, in the

Fe-free samples, OAc resulted in 18% of micropores merging into larger pores, which is half of that in the Fe-containing samples, that is, a 42% of micropores variation between the Fe/N/C(4mlm) and Fe/N/C(4mlm)-OAc catalysts (Table S1, Supporting Information). The result indicates that OAc is not the mere factor for the pore-merging process. A tenfold Fe content difference between OAc and OAc-free precursors at  $N_{\text{mlm}}/N_{\text{Zn}} = 4$  may also contribute to the pore-merging process owing to the catalytic effect of Fe on carbon decomposition (Figure S3, Supporting Information).<sup>[16]</sup> At a higher  $N_{\text{mlm}}/N_{\text{Zn}}$  value of 8, the Fe content difference between OAc and OAc-free precursors decreased to 1.5-fold, resulting in only 26% of micropores merging into larger pores in the resultant Fe/N/C catalysts (Figure 2e,f). Note that the external surface area of an Fe/N/C(8mlm)-OAc catalyst was only 0.46-fold that of the Fe/N/C(4mlm)-OAc catalyst (169 versus 365 m<sup>2</sup> g<sup>-1</sup>), despite a very similar Fe and OAc content in their pyrolysis precursors



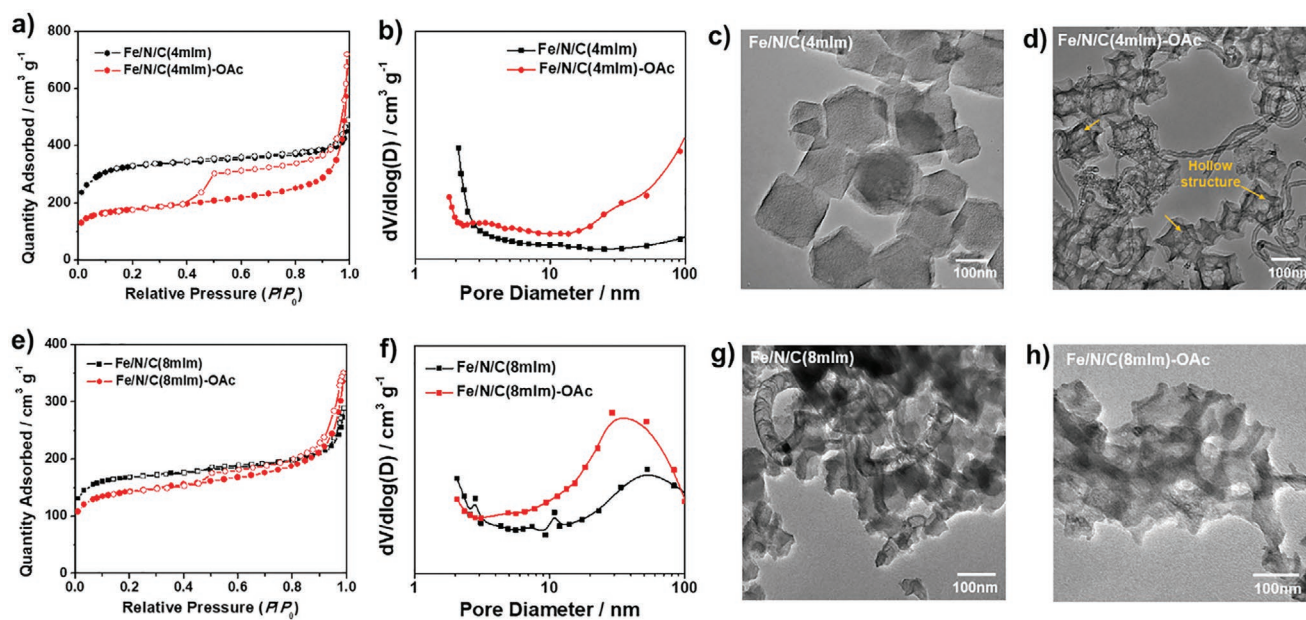


**Figure 2.** a)  $N_2$  adsorption–desorption isotherms and b) the corresponding pore size distribution of the Fe/N/C(4mlm) and Fe/N/C(4mlm)-OAc catalysts. c,d) TEM images of the (c) Fe/N/C(4mlm) and (d) Fe/N/C(4mlm)-OAc catalysts. e)  $N_2$  adsorption–desorption isotherms and f) the corresponding pore size distribution of Fe/N/C and Fe/N/C-OAc catalysts at  $N_{\text{mlm}}/N_{\text{zn}} = 8$ . g,h) TEM images of the (g) Fe/N/C(8mlm) and (h) Fe/N/C(8mlm)-OAc catalysts.

(Figure 1c,d). A lower mesoporosity in the Fe/N/C(8mlm)-OAc might be caused by a large-area agglomeration of ZIF-8 particles during the pyrolysis process due to rather tiny particle sizes (Figure S7, Supporting Information),<sup>[7b]</sup> as evidenced by the observation that the boundary between carbon particles disappeared in the Fe/N/C(8mlm) series catalysts (Figure 2g,h).

Another phenomenon that needed to be revealed is the occurrence of entangled CNTs and their dependence on OAc. By correlating three parameters, that is, the Fe content in the precursors (Figure S3, Supporting Information), crystalline Fe particles (Figure S10, Supporting Information), and CNTs in the pyrolysis products (Figure S11, Supporting Information), it was found that CNTs appeared only when the Fe content in the precursors was above 2 wt%, and their occurrence was accompanied with Fe/Fe<sub>2</sub>C<sub>5</sub> nanoparticles (Table S2, Supporting Information). This result suggests that the formation of CNTs is catalyzed by Fe nanoparticles,<sup>[16a]</sup> whose production is ensured by sufficient Fe content in the pyrolysis precursors. Although OAc is not directly correlated with CNTs, OAc can increase the Fe doping content in the ZIF-8 precursors, and in turn promote the formation of Fe/Fe<sub>2</sub>C<sub>5</sub> nanoparticles and CNTs. Note that these Fe nanoparticles were mainly covered by carbon layers. This point can be supported by an acid-leaching experiment with an Fe/N/C(4mlm)-OAc catalyst as an example. The Fe content of the Fe/N/C(4mlm)-OAc catalyst was determined to be 3.49 wt% by ICP-MS. After acid leaching by 0.5 M H<sub>2</sub>SO<sub>4</sub>, the total Fe content decreased to 3.24 wt% with below a 10% variation of Fe content (Figure S12, Supporting Information), in support of most of Fe species in the form of either atomically dispersed Fe sites or nanoparticles encapsulated within carbon layers.

By comparing the structure and property of ZIF-8 precursors and the resultant Fe/N/C catalysts with and without OAc, it is

concluded that the addition of OAc leads to a higher Fe doping content in the ZIF-8 precursors, a higher mesoporosity, and denser CNTs in the resultant Fe/N/C catalysts.

The ORR polarization curves of the Fe/N/C and Fe/N/C-OAc series catalysts were recorded by a rotating ring-disk electrodes (RRDE) test in O<sub>2</sub>-saturated 0.1 M H<sub>2</sub>SO<sub>4</sub> solution (Figures 3a,b). The mass activity of these catalysts at 0.85 V versus RHE were calculated through mass-transfer correction (Koutecky–Levich equation) and mass normalization (Figure 3c).<sup>[17]</sup> A higher mass activity corresponds to a higher intrinsic catalytic activity.<sup>[18]</sup> Without OAc, the intrinsic catalytic activity of Fe/N/C catalysts exhibited a volcanic variation with increasing  $N_{\text{mlm}}/N_{\text{zn}}$  values. At  $N_{\text{mlm}}/N_{\text{zn}} \leq 8$ , the increase of catalytic activity was attributed to the increasing Fe content (Figure 1c) and the decreasing particle size of ZIF precursors (Figure S7, Supporting Information).<sup>[6b,7b]</sup> However, too tiny particle sizes at  $N_{\text{mlm}}/N_{\text{zn}} = 10$  would lead to a large-area agglomeration of particles and a low mesoporosity (Figure S13, Supporting Information), decreasing the accessibility of active sites and the ORR activity.<sup>[19]</sup> After the addition of OAc, at least a twofold ORR activity improvement was observed at different  $N_{\text{mlm}}/N_{\text{zn}}$  values. At an optimized  $N_{\text{mlm}}/N_{\text{zn}}$  value of 4, the Fe/N/C-4mlm-OAc exhibited a mass activity of 5.98 A g<sup>-1</sup> at 0.85 V and 23.8 A g<sup>-1</sup> at 0.82 V versus RHE, exceeding most of the previously reported M/N/C ORR catalysts' (Table S3, Supporting Information). The intrinsic catalytic activity of ORR catalysts is highly dependent on the accessible active site density (SD). The SD was quantitated by a previously reported nitrite reduction method.<sup>[8,20]</sup> The nitrite anions were first adsorbed onto the FeN<sub>x</sub> active sites, then removed entirely through an electrochemical CV treatment (Figure 3d,e and Figure S14, Supporting Information). The number of active sites was presumed to be equal to how many nitrite anions were adsorbed. The

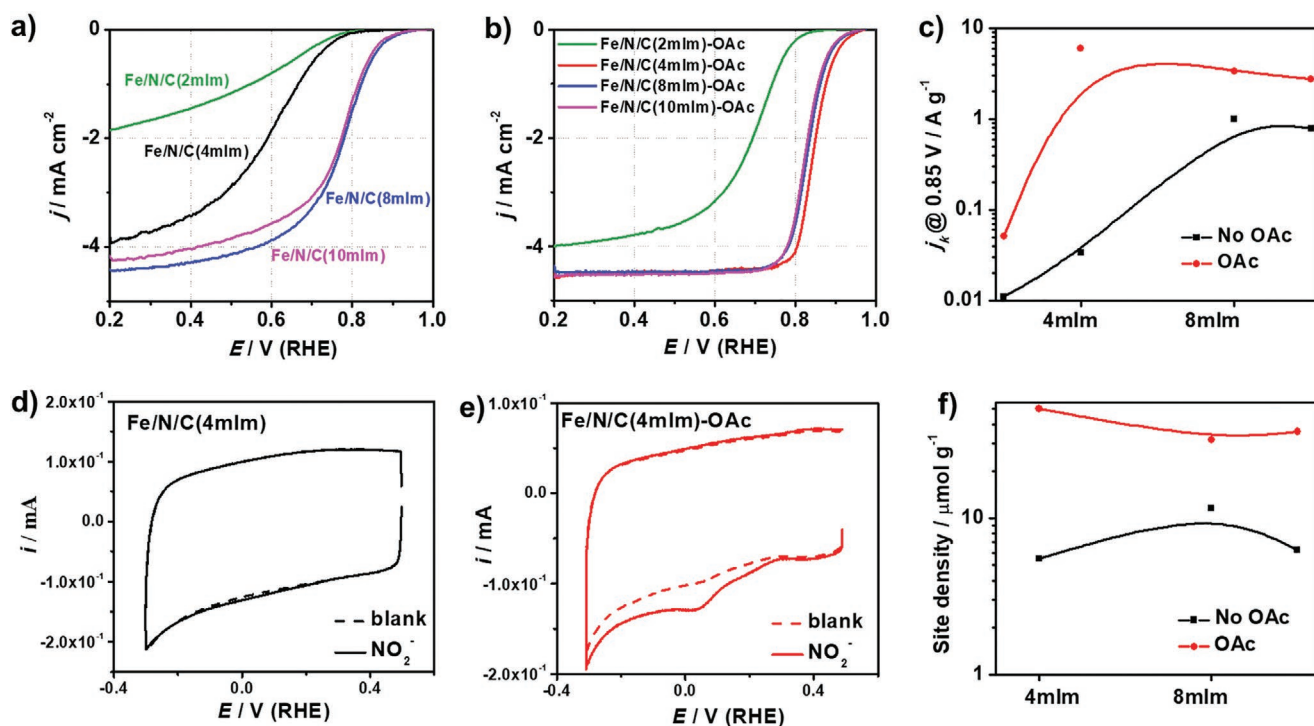


**Figure 3.** a,b) ORR polarization curves of (a) OAc-free Fe/N/C catalysts and (b) OAc-assisted Fe/N/C catalysts at different  $N_{\text{mlm}}/N_{\text{zn}}$ . Test conditions: O<sub>2</sub>-saturated 0.1 M H<sub>2</sub>SO<sub>4</sub>; Rotating speed: 900 rpm; Scan rate: 10 mV s<sup>-1</sup>; Catalyst loading: 0.6 mg cm<sup>-2</sup>; 30 °C water bath. c) A comparison of mass activity at 0.85 V (RHE) of Fe/N/C catalysts with and without OAc at different  $N_{\text{mlm}}/N_{\text{zn}}$ . d,e) CV curves of the (d) Fe/N/C(4mlm) and (e) Fe/N/C(4mlm)-OAc catalysts with and without nitrite adsorption for measurement of active sites density (SD). Solution: 0.5 M acetate buffer at pH 5.2; Catalyst loading, 0.27 mg cm<sup>-2</sup>. f) The comparison of Fe/N/C catalysts' SD with and without OAc at different  $N_{\text{mlm}}/N_{\text{zn}}$ . The SD values of Fe/N/C(2mlm) and Fe/N/C(2mlm)-OAc were not shown here because of a large measurement error of the method for Fe/N/C catalysts with low active site density.

latter could be calculated by integrating the charge of nitrite reduction. The detailed calculation equation was listed in the Experimental Section (Supporting Information). The specific SD values of all the catalysts were calculated and plotted in Figure 3f. Consistent with the ORR mass activity, the SD values of these catalysts showed a similar trend with at least 1.7-fold SD increment after the addition of OAc. This result suggests that the ORR activity improvement by OAc is mainly attributed to the increased SD, owing to a denser FeN<sub>x</sub> active site and a more open structure. A higher Fe content in the precursors tends to generate denser FeN<sub>x</sub> active sites in the resulting

Fe/N/C catalysts;<sup>[8]</sup> a higher mesoporosity can expose more sites accessible in the ORR.<sup>[21]</sup> Additionally, denser CNTs can also accelerate the charge-transfer process and increase the ORR activity by speeding up the electron delivery rate (Figure S15, Supporting Information).<sup>[7a,22]</sup>

OAc was the only one case of carboxylates. To demonstrate the generality of this strategy, three different forms of carboxylates (formate, oxalate, and tartrate) were further tested to examine their influence on the ORR activity of ZIF-based Fe/N/C catalysts. Figure 4a plots the ORR polarization curves of the resultant three catalysts and the previous OAc sample.

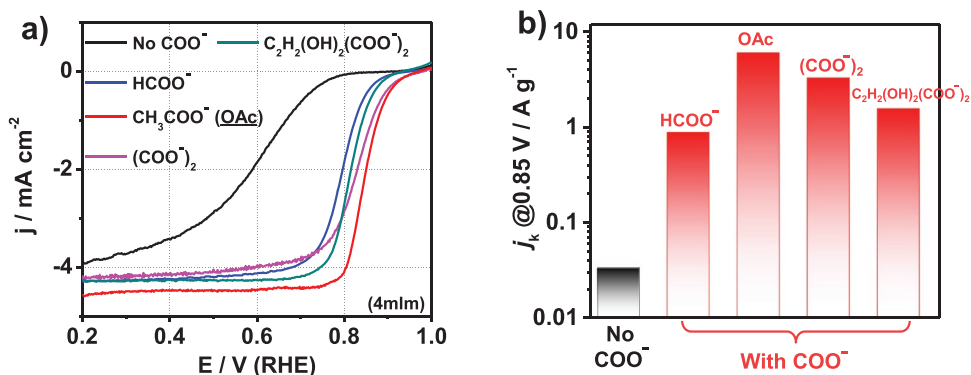


**Figure 4.** a) ORR polarization curves of Fe/N/C catalysts assisted by four different carboxylates at  $N_{\text{mlm}}/N_{\text{zn}} = 4$ . The control sample without OAc was also shown for comparison. b) The corresponding mass activity at 0.85 V (RHE) of the five Fe/N/C catalysts in (a).

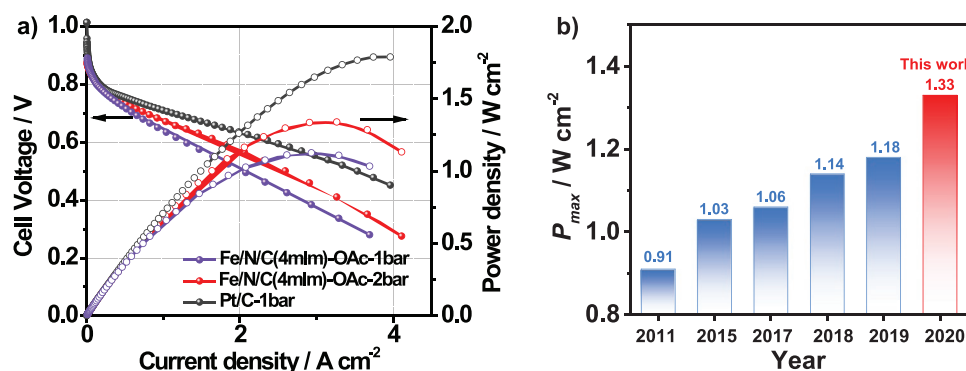


**Figure 5.** a) Polarization (left) and power density (right) curves of the H<sub>2</sub>-O<sub>2</sub> PEMFC with the Fe/N/C(4mlm)-OAc and commercial Pt/C catalyst as the cathode catalyst, respectively. Testing conditions: 1 or 2 bar backpressures; Flow rate: 0.3 slpm (H<sub>2</sub> and O<sub>2</sub>), MEA active area: 1.21 cm<sup>2</sup>; Nafion 211 membrane; Cathode loading: 3.0 mg cm<sup>-2</sup>; Anode catalyst: Pt/C (40 wt%, JM) with 0.4 mg<sub>pt</sub> cm<sup>-2</sup>; b) The growing P<sub>max</sub> of H<sub>2</sub>-O<sub>2</sub> PEMFCs with Fe/N/C catalyst as the cathode catalyst in recent years. The test conditions of the five ORR catalysts were listed in Table S4, Supporting Information.

The data of Fe/N/C catalyst without a carboxylate is also shown for comparison. Figure 4b compares the mass activity of these catalysts at 0.85 V versus RHE. The four carboxylate-assisted Fe/N/C catalysts showed an over tenfold ORR mass activity improvement and a twofold SD improvement relative to the reference sample (Figure S16, Supporting Information). Compared with the carboxylate-free sample, the four carboxylate-assisted samples exhibited a higher Fe doping content in the ZIF-8 precursors (Figure S17, Supporting Information), a higher mesoporosity (Figure S18, Supporting Information), and denser CNTs (Figure S19, Supporting Information) in the resultant Fe/N/C catalysts. This result implies the generality of the carboxylate-assisted method and the consistency of the mechanisms behind the ORR activity improvement. Although some literature has reported the section of carboxylate-containing Fe salts to synthesize M/N/C catalysts with superior ORR activity,<sup>[13,22b]</sup> the role of a carboxylate itself is rarely concerned.

To examine the practical performance of OAc-assisted Fe/N/C catalysts, we carried out an H<sub>2</sub>-O<sub>2</sub> PEMFC test with the best Fe/N/C(4mlm)-OAc catalyst as the cathode catalyst (Figure 5a). Owing to its high ORR mass activity, the loading of the Fe/N/C(4mlm)-OAc catalyst in the cathode decreased to 3 mg cm<sup>-2</sup> from a typical loading of 4 mg cm<sup>-2</sup>. The decrease of catalyst loading without compromising the activity will improve the mass transfer, or P<sub>max</sub>. At 1 bar backpressure, the Fe/N/C(4mlm)-OAc cathode generated a P<sub>max</sub> of 1.12 W cm<sup>-2</sup> at 0.38 V. At a higher backpressure of 2 bar, the P<sub>max</sub> increased to 1.33 W cm<sup>-2</sup>, and good reproducibility of the high power density was demonstrated through repeated experiments (Figure S20, Supporting Information). To the best of our knowledge, this is the highest P<sub>max</sub> reported in a H<sub>2</sub>-O<sub>2</sub> PEMFC so far with M/N/C catalysts as cathode catalysts (Figure 5b and Table S4, Supporting Information). In PEMFC, air is more practical than oxygen. Therefore, a H<sub>2</sub>-air PEMFC was tested. As shown in Figure S21, Supporting Information, the Fe/N/C(4mlm)-OAc cathode generated a peak power density of 467 and 538 mW cm<sup>-2</sup> at 1 and 2 bar backpressures, respectively.

The superior P<sub>max</sub> of the Fe/N/C(4mlm)-OAc cathode was mainly achieved by three factors, that is, high kinetic activity,

low internal resistance, and fast mass transfer.<sup>[3b,8,17,23]</sup> A high density of accessible active sites of the Fe/N/C(4mlm)-OAc catalyst ensured the high kinetic activity of the cathode. Quantitatively, the cathode generated a current density of 9.3 mA cm<sup>-2</sup> at 0.9 V<sub>iR-free</sub> (Figure S22, Supporting Information). A large number of entangled CNTs in the Fe/N/C(4mlm)-OAc accelerated the cathode's electron transport, lowering the internal resistance of a whole-cell (Figure S23, Supporting Information).<sup>[3b,22b]</sup> The high mesoporosity of the Fe/N/C(4mlm)-OAc catalyst, coupled with the decreased cathode catalyst loading, speeded up the cathode's mass transfer. Although an unprecedented P<sub>max</sub> was achieved among M/N/C cathodes, however, it was still somehow lower than that of the Pt/C cathode (1.8 W cm<sup>-2</sup>, 1 bar backpressure). More work should be done to fill this gap in the future.

The stability of the Fe/N/C(4mlm)-OAc catalyst was tested in a H<sub>2</sub>-O<sub>2</sub> PEMFC with the cell voltage holding at 0.5 V. As shown in Figure S24, Supporting Information, the Fe/N/C(4mlm)-OAc showed an 80.3% of activity loss in the initial 35 h. More work should be done to improve the poor stability of active Fe/N/C catalysts.

### 3. Conclusion

In summary, the carboxylate-assisted synthesis of Fe/N/C catalysts was demonstrated as a general approach to boost the ORR activity of ZIF-derived Fe/N/C catalysts by increasing the density of accessible active sites and the amount of CNTs as well as mesoporosity. Upon optimization of Fe/N/C as a cathode catalyst, the H<sub>2</sub>-O<sub>2</sub> PEMFC generated a record-high peak power density up to 1.33 W cm<sup>-2</sup>. Our strategy will help develop high-performance, cost-effective M/N/C ORR catalysts, especially MOFs-based catalytic materials.

### Supporting Information

Supporting Information is available from the Wiley Online Library or from the author.



## Acknowledgements

This work was supported by grants from the National Key Research and Development Program of China (2016YFB0101200) and Natural Science Foundation of China (21875194). J.Y. thanks for the Wallenberg Academy Fellow program (WAF2017.0166) from the Knut and Alice Foundation in Sweden. Special statement: The authors Y.S.W. and K.Z. have nothing to do with the program, and they are not supported by the program.

## Conflict of Interest

The authors declare no conflict of interest.

## Data Availability Statement

Research data are not shared.

## Keywords

carboxylate, Fe/N/C catalysts, fuel cells, metal–organic frameworks, oxygen reduction reaction

Received: November 12, 2020

Revised: December 21, 2020

Published online: February 8, 2021

- [1] a) M. Lefevre, E. Proietti, F. Jaouen, J. P. Dodelet, *Science* **2009**, 324, 71; b) G. Wu, K. L. More, C. M. Johnston, P. Zelenay, *Science* **2011**, 332, 443; c) H. T. Chung, D. A. Cullen, D. Higgins, B. T. Sneed, E. F. Holby, K. L. More, P. Zelenay, *Science* **2017**, 357, 479.
- [2] a) N. R. Sahraie, U. I. Kramm, J. Steinberg, Y. Zhang, A. Thomas, T. Reier, J. P. Paraknowitsch, P. Strasser, *Nat. Commun.* **2015**, 6, 8618; b) L. Zhao, Y. Zhang, L. B. Huang, X. Z. Liu, Q. H. Zhang, C. He, Z. Y. Wu, L. J. Zhang, J. Wu, W. Yang, L. Gu, J. S. Hu, L. J. Wan, *Nat. Commun.* **2019**, 10, 1278; c) X. Yang, C. Chen, Z. Zhou, S. Sun, *Acta Phys.-Chim. Sin.* **2019**, 35, 472.
- [3] a) E. Proietti, F. Jaouen, M. Lefevre, N. Larouche, J. Tian, J. Herranz, J. P. Dodelet, *Nat. Commun.* **2011**, 2, 416; b) X. Fu, P. Zamani, J. Y. Choi, F. M. Hassan, G. Jiang, D. C. Higgins, Y. Zhang, M. A. Hoque, Z. Chen, *Adv. Mater.* **2017**, 29, 1604456; c) Y. He, S. Hwang, D. A. Cullen, M. A. Uddin, L. Langhorst, B. Li, S. Karakalos, A. J. Kropf, E. C. Wegener, J. Sokolowski, M. Chen, D. Myers, D. Su, K. L. More, G. Wang, S. Litster, G. Wu, *Energy Environ. Sci.* **2019**, 12, 250.
- [4] X. Yang, Y. Wang, G. Zhang, L. Du, L. Yang, M. Markiewicz, J. y. Choi, R. Chenitz, S. Sun, *Appl. Catal., B* **2020**, 264, 118523.
- [5] a) J. Li, M. Chen, D. A. Cullen, S. Hwang, M. Wang, B. Li, K. Liu, S. Karakalos, M. Lucero, H. Zhang, *Nat. Catal.* **2018**, 1, 935; b) Z. Yang, C. Zhao, Y. Qu, H. Zhou, F. Zhou, J. Wang, Y. Wu, Y. Li, *Adv. Mater.* **2019**, 31, 1808043.
- [6] a) J. Wang, Z. Huang, W. Liu, C. Chang, H. Tang, Z. Li, W. Chen, C. Jia, T. Yao, S. Wei, Y. Wu, Y. Li, *J. Am. Chem. Soc.* **2017**, 139, 17281; b) H. Zhang, H. T. Chung, D. A. Cullen, S. Wagner, U. I. Kramm, K. L. More, P. Zelenay, G. Wu, *Energy Environ. Sci.* **2019**, 12, 2548; c) J. Li, L. Jiao, E. Wegener, L. L. Richard, E. Liu, A. Zitolo, M. T. Sougrati, S. Mukerjee, Z. Zhao, Y. Huang, F. Yang, S. Zhong, H. Xu, A. J. Kropf, F. Jaouen, D. J. Myers, Q. Jia, *J. Am. Chem. Soc.* **2020**, 142, 1417.
- [7] a) B. Y. Xia, Y. Yan, N. Li, H. B. Wu, X. W. Lou, X. Wang, *Nat. Energy* **2016**, 1, 15006; b) H. Zhang, S. Hwang, M. Wang, Z. Feng, S. Karakalos, L. Luo, Z. Qiao, X. Xie, C. Wang, D. Su, Y. Shao, G. Wu, *J. Am. Chem. Soc.* **2017**, 139, 14143; c) J. Li, H. Zhang, W. Samarakoon, W. Shan, D. A. Cullen, S. Karakalos, M. Chen, D. Gu, K. L. More, G. Wang, *Angew. Chem.* **2019**, 131, 18971.
- [8] X. Wan, X. Liu, Y. Li, R. Yu, L. Zheng, W. Yan, H. Wang, M. Xu, J. Shui, *Nat. Catal.* **2019**, 2, 259.
- [9] a) J. Tian, A. Morozan, M. T. Sougrati, M. Lefèvre, R. Chenitz, J. P. Dodelet, D. Jones, F. Jaouen, *Angew. Chem., Int. Ed.* **2013**, 52, 6867; b) Q. Lai, L. Zheng, Y. Liang, J. He, J. Zhao, J. Chen, *ACS Catal.* **2017**, 7, 1655.
- [10] Y. Luo, S. Fan, W. Yu, Z. Wu, D. A. Cullen, C. Liang, J. Shi, C. Su, *Adv. Mater.* **2018**, 30, 1704576.
- [11] a) R. Hong, T. Pan, J. Qian, H. Li, *Chem. Eng. J.* **2006**, 119, 71; b) J. Li, Q. Zhang, J. Liu, M. Yu, H. Ma, J. Yang, S. Ye, T. Ramirez Reina, J. Liu, *J. Colloid Interface Sci.* **2020**, 577, 512.
- [12] a) J. Cravillon, S. Münzer, S. J. Lohmeier, A. Feldhoff, K. Huber, M. Wiebcke, *Chem. Mater.* **2009**, 21, 1410; b) G. C. Shearer, S. Chavan, J. Ethiraj, J. G. Vitillo, S. Svelle, U. Olsbye, C. Lambert, S. Bordiga, K. P. Lillerud, *Chem. Mater.* **2014**, 26, 4068.
- [13] Y. Ye, F. Cai, H. Li, H. Wu, G. Wang, Y. Li, S. Miao, S. Xie, R. Si, J. Wang, X. Bao, *Nano Energy* **2017**, 38, 281.
- [14] a) J. Cravillon, C. A. Schröder, H. Bux, A. Rothkirch, J. Caro, M. Wiebcke, *CrystEngComm* **2012**, 14, 492; b) J. Cravillon, R. Nayuk, S. Springer, A. Feldhoff, K. Huber, M. Wiebcke, *Chem. Mater.* **2011**, 23, 2130.
- [15] D. Liu, J. C. Li, S. Ding, Z. Lyu, S. Feng, H. Tian, C. Huan, M. Xu, T. Li, D. Du, P. Liu, M. Shao, Y. Lin, *Small Methods* **2020**, 4, 1900827.
- [16] a) X. Wang, Q. Li, H. Pan, Y. Lin, Y. Ke, H. Sheng, M. T. Swihart, G. Wu, *Nanoscale* **2015**, 7, 20290; b) Z. L. Yu, S. Xin, Y. You, L. Yu, Y. Lin, D. W. Xu, C. Qiao, Z. H. Huang, N. Yang, S. H. Yu, J. B. Goodenough, *J. Am. Chem. Soc.* **2016**, 138, 14915.
- [17] Y. C. Wang, Y. J. Lai, L. Song, Z. Y. Zhou, J. G. Liu, Q. Wang, X. D. Yang, C. Chen, W. Shi, Y. P. Zheng, M. Rauf, S. G. Sun, *Angew. Chem., Int. Ed.* **2015**, 54, 9907.
- [18] Q. Wang, Z. Y. Zhou, Y. J. Lai, Y. You, J. G. Liu, X. L. Wu, E. Terefe, C. Chen, L. Song, M. Rauf, N. Tian, S. G. Sun, *J. Am. Chem. Soc.* **2014**, 136, 10882.
- [19] A. Uddin, L. Dunsmore, H. Zhang, L. Hu, G. Wu, S. Litster, *ACS Appl. Mater. Interfaces* **2020**, 12, 2216.
- [20] a) D. Malko, A. Kucernak, T. Lopes, *Nat. Commun.* **2016**, 7, 13285; b) M. Primbs, Y. Sun, A. Roy, D. Malko, A. Mehmood, M. T. Sougrati, P. Y. Blanchard, G. Granozzi, T. Kosmala, G. Daniel, P. Atanassov, J. Sharman, C. Durante, A. Kucernak, D. Jones, F. Jaouen, P. Strasser, *Energy Environ. Sci.* **2020**, 13, 2480.
- [21] a) W. Shi, Y. C. Wang, C. Chen, X. D. Yang, Z. Y. Zhou, S. G. Sun, *Chin. J. Catal.* **2016**, 37, 1103; b) L. Shang, H. Yu, X. Huang, T. Bian, R. Shi, Y. Zhao, G. I. N. Waterhouse, L. Z. Wu, C. H. Tung, T. Zhang, *Adv. Mater.* **2016**, 28, 1712; c) L. Jiao, G. Wan, R. Zhang, H. Zhou, S. H. Yu, H. L. Jiang, *Angew. Chem., Int. Ed.* **2018**, 57, 8525.
- [22] a) C. Zhang, Y. C. Wang, B. An, R. Huang, C. Wang, Z. Zhou, W. Lin, *Adv. Mater.* **2017**, 29, 1604556; b) W. Li, W. Ding, Y. Nie, Q. He, J. Jiang, Z. Wei, *ACS Appl. Mater. Interfaces* **2019**, 11, 22290.
- [23] a) Y. C. Wang, L. Huang, P. Zhang, Y. T. Qiu, T. Sheng, Z. Y. Zhou, G. Wang, J. G. Liu, M. Rauf, Z. Q. Gu, W. T. Wu, S. G. Sun, *ACS Energy Lett.* **2017**, 2, 645; b) Y. C. Wang, P. F. Zhu, H. Yang, L. Huang, Q. H. Wu, M. Rauf, J. Y. Zhang, J. Dong, K. Wang, Z. Y. Zhou, S. G. Sun, *ChemElectroChem* **2018**, 5, 1914; c) Q. Liu, X. Liu, L. Zheng, J. Shui, *Angew. Chem., Int. Ed.* **2018**, 57, 1204.